AGU PUBLICATIONS

Geophysical Research Letters

RESEARCH LETTER
10.1002/2017GL076406

Key Points:
- The unprecedented disruption in 2016 of the QBO was successfully captured in a series of 40 day ensemble hindcasts
- The QBO disruption is caused by the interaction of Rossby waves of extratropical origin with the equatorial mean flow
- The individual ensemble members displayed quite similar equatorial mean wind evolution despite large differences in the extratropics

Correspondence to:
S. Watanabe,
wnabe@jamstec.go.jp

Citation:
Watanabe, S., Hamilton, K., Osprey, S., Kawatani, Y., & Nishimoto, E. (2018). First successful hindcasts of the 2016 disruption of the stratospheric quasi-biennial oscillation. *Geophysical Research Letters*, *45*, 1602–1610. https://doi.org/10.1002/2017GL076406

Received 14 NOV 2017
Accepted 21 DEC 2017
Accepted article online 29 DEC 2017
Published online 2 FEB 2018

The copyright line for this article was changed on 11 JUL 2018 after original online publication

First Successful Hindcasts of the 2016 Disruption of the Stratospheric Quasi-biennial Oscillation

S. Watanabe[1], K. Hamilton[2], S. Osprey[3], Y. Kawatani[1], and E. Nishimoto[1]

[1]Japan Agency for Marine-Earth Science and Technology, Yokohama, Japan, [2]International Pacific Research Center, University of Hawai'i at Mānoa, Honolulu, HI, USA, [3]NCAS-Climate, University of Oxford, Oxford, UK

Abstract In early 2016 the quasi-biennial oscillation in tropical stratospheric winds was disrupted by an anomalous easterly jet centered at ~40 hPa, a development that was completely missed by all operational extended range weather forecast systems. This event and its predictability are investigated through 40 day ensemble hindcasts using a global model notable for its sophisticated representation of the upper atmosphere. Integrations starting at different times throughout January 2016—just before and during the initial development of the easterly jet—were performed. All integrations simulated the unusual developments in the stratospheric mean wind, despite considerable differences in other aspects of the flow evolution among the ensemble members, notably in the evolution of the winter polar vortex and the day-to-day variations in extratropical Rossby waves. Key to prediction of this event is simulating the slowly evolving mean winds in the winter subtropics that provide a waveguide for Rossby waves propagating from the winter hemisphere.

Plain Language Summary In early 2016 the regular winds high up in the tropical atmosphere were disturbed in a way not seen in over 60 years of observations. The usual regularity of the year-to-year changes in these winds contributes to skillful long range weather forecasts worldwide, so when weather centers failed to pick up this event, predictions of seasonal weather were affected. This study reports a successful retrospective forecast of the 2016 disruption event using a global climate model notable for its detailed representation of the upper atmosphere and provides a benchmark for future forecast models. It has been found that dramatic changes to the high-latitude winds in the upper atmosphere had little influence on the development of the tropical anomaly, but rather the distribution of prevailing winds closer to the tropics was crucially important.

1. Introduction

The quasi-biennial oscillation (QBO) in the equatorial lower stratosphere is characterized by quasi periodic reversals of the zonal mean easterly and westerly winds. The QBO wind reversals descend in height and each complete cycle takes between 22 to 34 months with a long-term average period of approximately 28 months (e.g., Baldwin et al., 2001). The mean wind accelerations driving the QBO are thought to largely result from interactions of the mean zonal wind with vertically propagating internal waves generated in the tropical troposphere (Baldwin et al., 2001). These wave interactions will produce descending mean flow regimes, and the observed descent rate of the QBO phase depends on a balance between this wave forcing and a competing mean upwelling in the tropical stratosphere. The long timescale and quasi-regular periodicity potentially allow seasonal to decadal prediction of the QBO, and this has practical implications as the QBO in the tropical stratosphere is correlated with seasonal weather patterns at the surface, particularly over the North Atlantic and Europe in winter (Boer & Hamilton, 2008; Marshall & Scaife, 2009). In fact, the situation with forecasts of the QBO is somewhat paradoxical—coupled atmosphere-ocean model forecast systems have shown skillful forecasts well beyond seasonal time scales (Scaife et al., 2014), but this skill can be matched by assuming a simple sinusoidal wind variation of constant 28 month period (Scaife et al., 2014). The real challenge for forecast models is extending the lead time for skillful predictions of the QBO and also to test whether variations from mean cycling are predictable, and this kind of test has not been demonstrated thus far. This issue has recently taken center stage as—for the first time in our >60 year observation record—a major disruption of the usual QBO cycle occurred. Specifically during the boreal winter 2015/2016, an anomalous easterly wind layer developed in the middle of the QBO westerly winds (Newman et al., 2016; Osprey et al., 2016). Diagnosis of observations during the event suggest the development of the anomalous easterly wind layer was caused by unprecedentedly strong wave forcing of the mean zonal winds due to upward and southward

propagating planetary-scale Rossby waves originating from the Northern Hemisphere (Coy et al., 2017; Osprey et al., 2016). The extreme and unprecedented nature of the tropical stratospheric and surrounding winds during 2015/2016 was discussed by Dunkerton (2016).

Strikingly none of the operational seasonal forecasting centers have subsequently reported reproducing the 2016 disruption of the QBO, instead forecasting a very typical development of the QBO through this period (e.g., Osprey et al., 2016). The realistic simulation of the QBO has long been recognized as a particular problem for general circulation models (GCMs), and most current models that produce a reasonable QBO in the tropical stratosphere (including all currently used in the operational forecast centers) employ rather highly tuned parameterizations of the component of the mean flow forcing due to unresolved waves (Schenzinger et al., 2017). The experience in 2016 suggests that such models may not be able to adequately represent the range of QBO variability. This in turn suggests that they will not be able to capitalize on the full potential for skillful extended range weather prediction inherent in the stratospheric QBO.

Here for the first time we investigate the predictability of the 2015/2016 QBO disruption, using a high-vertical resolution atmospheric GCM capable of spontaneously generating QBO-like oscillations (Kawatani et al., 2010a, 2010b; Watanabe et al., 2008). We focus on the January–February 2016 period during which the anomalous easterly wind layer developed and the Rossby wave forcing was strongest in the observational record and perform several ensemble 40 day hindcast experiments. We will show that our model is able to successfully hindcast the unusual tropical stratospheric mean winds during the development of the disruption. The successful hindcast ensembles will then be analyzed to try to establish the key mechanisms in the development of the disruption and the implications for extended range predictability of the QBO winds. The model and experimental design are described in section 2, followed by an analysis of results in section 3 and a summary of conclusions in section 4.

2. Model and Experimental Design

The model used in the present study is JAGUAR (Japanese Atmospheric General circulation model for Upper Atmosphere Research; Watanabe & Miyahara, 2009). The vertical domain of this model extends from the Earth's surface to a height of around 150 km. The horizontal resolution is set to 0.56°, which is the same as that used by Watanabe et al. (2008) and Watanabe and Miyahara (2009). This horizontal resolution allows the model to resolve gravity waves with horizontal wavelengths larger than ~190 km. Although the present model cannot resolve the full range of observed gravity waves, it nonetheless produces fairly realistic behavior of the QBO winds, without resort to nonorographic gravity wave parameterizations (Kawatani et al., 2010a, 2010b; Watanabe et al., 2008). The vertical grid resolution above about 8 km altitude is set to 300 m as in Watanabe et al. (2015). Such fine vertical resolution may be needed for simulating the abnormal QBO behavior in January–February 2016 given the small vertical scale of the observed disruption in the mean winds.

The JAGUAR model has been developed for free running simulations of the middle and upper atmosphere circulation and has not previously been applied to forecasting. In this project ensembles of 40 day hindcast simulations were performed with initial conditions spaced at 1 week intervals: 4, 11, 18, and 25 January and 1 February 2016. Each hindcast is proceeded by a 24 h period during which the model's zonal and meridional winds, temperature, and specific humidity are strongly relaxed to the Modern-Era Retrospective Analysis for Research and Applications, version 2 (MERRA-2) three-hourly instantaneous model-level assimilated fields (Global Modeling and Assimilation Office, 2015) producing the initial conditions for the hindcast. An array of different initial conditions for the ensemble hindcast experiments were generated by slightly changing the relaxation time constant. Note that the model simply ran freely above the 0.01 hPa level where the MERRA-2 data were not available.

The ensemble for each hindcast was expanded to include multiple physics members. Specifically, we ran three versions each with different values of the critical relative humidity (*RHc*) parameter in the model prognostic-type Arakawa Schubert cumulus parameterization (Emori et al., 2001). The RHc parameter defines a threshold of cloud-mean air moisture for triggering cumulus convection. A larger value of RHc generally results in the higher intermittency and stronger horizontal aggregation of parameterized precipitation in the model. In the present study, we choose three plausible values for RHc (0.6, 0.72, and 0.8) which are

each applied to the nine-member initial condition ensemble. The combined physics parameter (×3) and initial condition ensemble (×9) for each hindcast experiment has 27 members.

Observed daily sea surface temperatures (SST) and sea ice concentration taken from Optimum Interpolation Sea Surface Temperature (OISST) (Banzon et al., 2016), and the zonal mean value of monthly ozone climatology (Li & Shine, 1999) were prescribed in the hindcast experiments.

Model output included daily averaged three-dimensional winds and temperatures and the internally calculated two-dimensional zonal mean variables required in the transformed Eulerian mean (TEM) diagnostics (cf. Andrews et al., 1987), including contributions of the subdaily and total-horizontal-wave components (labeled as "Total-Waves"). Planetary and synoptic-scale features, including breaking Rossby waves, are extracted by applying a low-pass filter of zonal wave number 1–20 to the daily averaged three-dimensional output (labeled as "Large-Waves"). The remaining subdaily and small-scale wave components ("Small-Waves") in the TEM diagnostics, principally explicitly resolved gravity waves, are obtained by subtracting the Large-Waves from the Total-Waves.

3. Results

3.1. Vertical Profiles of the Equatorial Mean Zonal Winds

Figure 1 shows vertical profiles of the equatorial zonal mean zonal winds, $\overline{u}$, plotted at 1 week intervals. The individual 27 ensemble members are plotted along with the MERRA-2 profiles; the colors indicating different initial dates (red: 4 January, blue: 11 January, green: 18 January, orange: 25 January, and cyan: 1 February) and the line intensity indicating the value of RHc (light: 0.6, medium: 0.72 and dark: 0.8). Note that even in the earliest initial state (4 January), the gradual weakening of the westerly wind, which leads to the development of the thin easterly wind layer near 40 hPa, is apparent. It is still striking how well the hindcasts then simulate the further development of the easterly layer and, more generally, the observed evolution of equatorial $\overline{u}$ in the 30–60 hPa layer. The ensembles initialized on 4 January and 1 February agree particularly well with the MERRA-2 within 30–60 hPa. On the other hand, the model had difficulty in reproducing the enhancement of the westerly wind peaks near 20 hPa and 70 hPa, which is a common feature among all the initial conditions. Notably, the model does not reproduce the very unusual upward progression of the westerly wind peak near 20 hPa. This upward progression was ascribed by Coy et al. (2017) to a vertical tropical upwelling that was anomalously strong above 40 hPa in the December 2015 to February 2016 period (at least in MERRA-2 reanalyses). Another potential mechanism would be the new shear zones formed below 20 hPa that will filter the waves and remove forcing from the shear zones above, leading to upward progression due to vertical advection. In all the simulations, the spread among the $\overline{u}$ profiles among the ensemble members is generally larger above 30 hPa than in the 30–60 hPa range. Notably, the hindcasts of $\overline{u}$ at 10–20 hPa tend to separate according to the RHc physics parameter employed with larger RHc values (darker colors) correlated with faster descent of the overlying easterly wind shear zone (see a magnified view in Figure 1a), suggesting that larger critical moisture thresholds in the convection parameterization lead to strong gravity wave forcing of these levels. The hindcasts of the equatorial $\overline{u}$ below 60 hPa are also generally less successful than the in the 30–60 hPa layer. The development of the lower 70 hPa QBO westerly wind peak is notably more poorly represented in the hindcasts initialized on 11 January (blue) and 18 January (green). The hindcasts initialized on 11 and 18 January also have the poorest performance in the easterly jet region near 40 hPa as well. The reason for the less successful forecasts initialized at these times is a subject for future study. Hereafter, our focus will be on the hindcasts initialized on 4 January (red) and 1 February (cyan) which seem to have the best overall representation of the equatorial $\overline{u}$, and we will investigate the factors that led to the development of the 40 hPa easterly layer in these relatively successful simulations.

3.2. Associations to the Extratropics

Figure 2 shows the ensemble mean and spread of $\overline{u}$ at forecast days 7, 14, 21, and 28 for the 4 January (red) and 1 February (cyan) ensembles. The ensemble spread of $\overline{u}$ remains very small in the equatorial lower stratosphere but grows rapidly near the tropospheric subtropical jets and the Northern Hemisphere (NH) polar vortex. Some members forecast the occurrence of a sudden stratospheric warming event, while others forecast the opposite—polar vortex intensification (not shown). Nevertheless, all the members successfully predicted

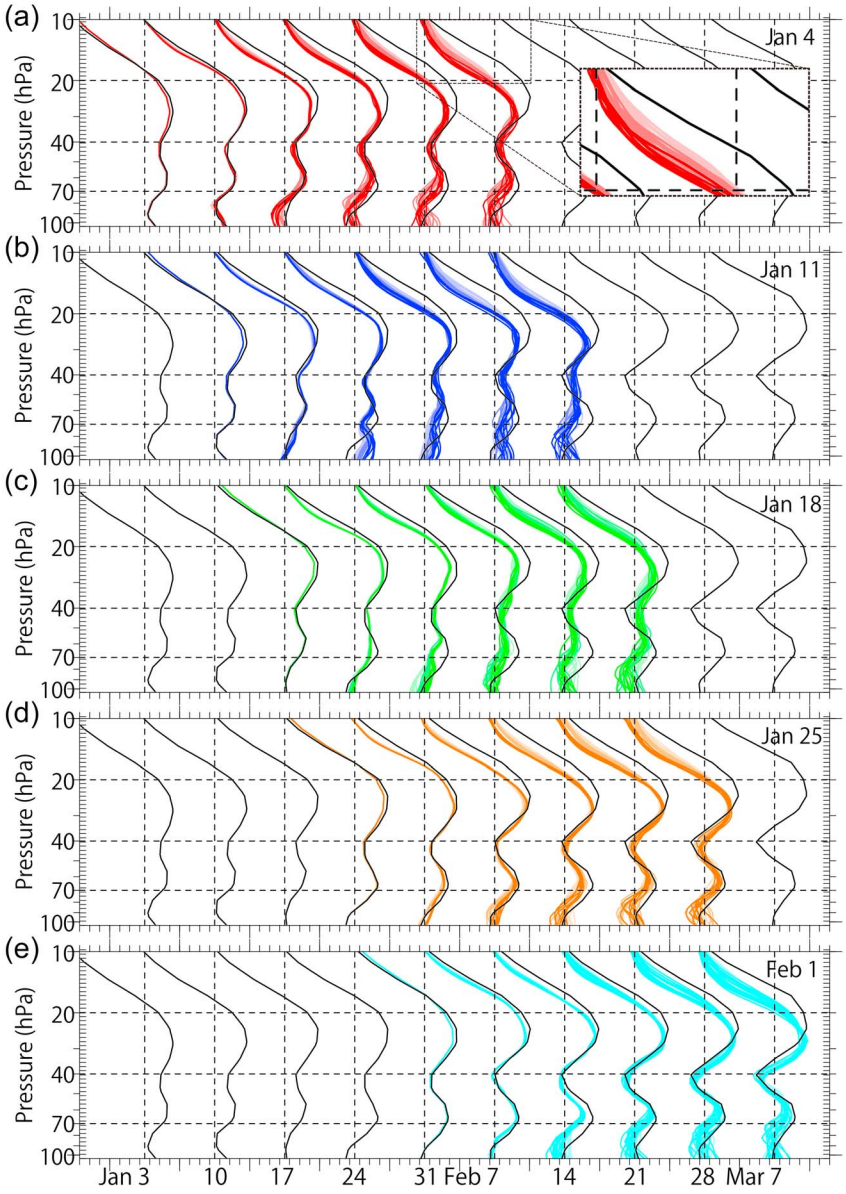

Figure 1. Vertical profiles of the equatorial (2°N–2°S) zonal mean zonal wind with 1 week interval from 3 January 2016 to 7 March 2016. The individual 27 ensemble members were plotted along with the MERRA-2 profiles (black curves). The different initial dates are indicated by colors (red: 4 January, blue: 11 January, green: 18 January, orange: 25 January, and cyan: 1 February), and the value of RHc by changing saturation (light: 0.6, medium: 0.72, and dark: 0.8). The 1 week interval, indicated by vertical dotted lines, corresponds to 28 m s^{-1} of zonal winds.

the development of the 40 hPa easterly wind layer in the QBO (red and cyan curves in Figure 1 and the contours in Figure 2).

Figure 3 shows the ensemble mean $\overline{u}$, Eliassen-Palm (E-P) flux arrows, and eastward dynamical accelerations due to meridional and vertical contributions to the E-P flux divergence, averaged over 4–24 January and 1–21 February. The Large-Waves, presumably dominated by quasi-stationary planetary Rossby waves, propagated southward from the NH subtropics to the Southern Hemisphere (SH) flank of the QBO and generated easterly wind accelerations near 40 hPa. Meanwhile, the Small-Waves consisting of small-scale gravity waves did not generate significant $\overline{u}$ accelerations near 40 hPa and act, as usual, to enhance the descent of vertical shears of $\overline{u}$ associated with the QBO. This assessment of the mean flow forcing generating the 40 hPa easterly wind layer based on our model hindcasts that explicitly simulate the wave fields agrees qualitatively with previous studies (Coy et al., 2017; Osprey et al., 2016) based on observational reanalyses.

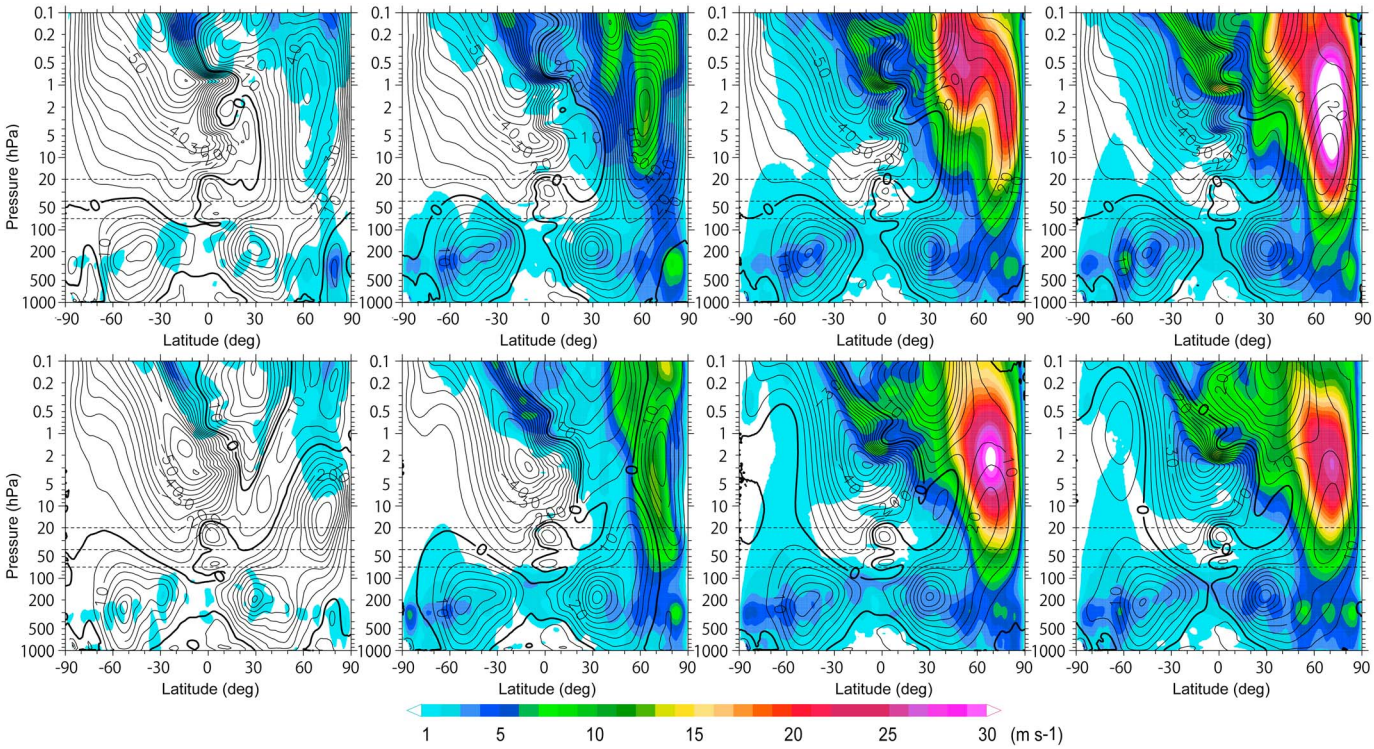

Figure 2. Ensemble mean (contours) and ensemble spread (shading) of the zonal mean zonal wind. The shading with less (greater) than 1 m s^{-1} (30 m s^{-1}) is suppressed. (top row) Time goes from left to right: days 7, 14, 21, and 28 from the 4 January initial conditions. (bottom row) Similar but those for the 1 February.

3.3. Predictability of Rossby Wave Activity

The dynamical analysis in the previous subsection confirms the importance of southward propagating Rossby waves on the development of the 40 hPa easterly wind layer in the QBO, based on the 3 week mean view. Coy et al. (2017) showed near 40 hPa potential vorticity maps in January–February 2016, which highlight the presence of transient wave structures in the tropics. Here we examine the day-to-day variations in the equatorial Rossby wave activity in our hindcasts.

Figure 4 shows daily time series of the meridional flux of zonal momentum at 40 hPa of 10°N, which is associated with the Large-Waves and compared with values computed from MERRA-2 reanalyses. There was some tendency for the ensemble members to agree over the first 10 days or so, but the ensemble spread grew rapidly afterward. The different values of RHc altered the day-to-day variations during the first 1 to 2 weeks, but no systematic difference in the Rossby waves could be found at later times. The largest wave event in early February was only captured by the 1 February initial condition ensemble, which is consistent with the particularly skillful forecasts in that ensemble (Figure 1). In summary, the model somehow reproduced the overall effect of the planetary Rossby waves on the development of the equatorial mean flow near 40 hPa, but not the day-to-day Rossby wave variations. The $\overline{u}$ in the stratosphere acts as an integrator of the forcing from waves, and this aspect of the circulation may be somewhat independent of the day-to-day wave variations.

3.4. Role of Rossby Waveguide

Through the dynamical analyses we have conducted in the previous subsections, we might conclude that forecasting variations in the northern polar vortex and individual wave events in the tropical lower stratosphere was not a necessary condition for the abnormal development of the near 40 hPa easterly wind layer in the model. Our current hypothesis is that the proximate source of predictability of the equatorial $\overline{u}$ near 40 hPa in January–February 2016 might come from slowly evolving waveguide structures in the tropical and NH subtropical lower stratosphere, including the QBO winds.

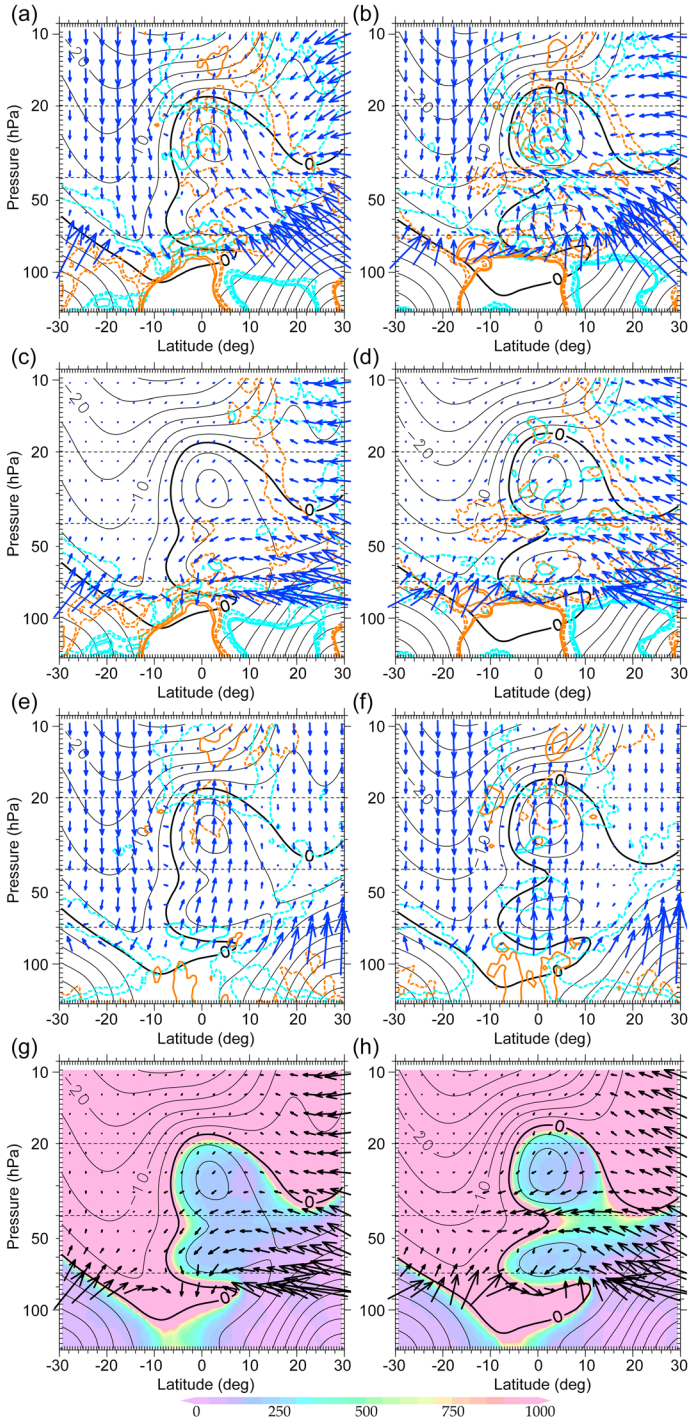

Figure 3. The ensemble-mean zonal mean zonal winds (black contours with a 5 m s^{-1} interval), E-P flux (arrows), and eastward dynamical accelerations due to the meridional (orange) and vertical (cyan) contributions to the divergence of the E-P flux components. The orange and cyan contours show only two levels for clarity, that is, ±5 m s^{-1} $month^{-1}$ and ±10 m s^{-1} $month^{-1}$, and the solid and dotted contours show positive and negative values, respectively. (a and b) The E-P flux and dynamical forcing associated with all wave components (Total-Waves). (c and d) Those associated with the daily averaged zonal wave number 1–20 wave components, which are dominated by Rossby waves (Large-Waves). (e and f) Those associated with subdaily and higher zonal wave number components, which are dominated by vertically propagating gravity waves (Small-Waves). (g and h) As in Figures 3c and 3d but shading represents the squared refractive index ($a^2 n_0^2$) for the zonal wave number 1–2 stationary Rossby waves (regions of negative values and values greater than 10^3 are saturated). Here a denotes the radius of the Earth. Figures 3a, 3c, 3e, and 3g, and 3b, 3d, 3f, and 3h show averages of 4–24 January and 1–21 February, respectively.

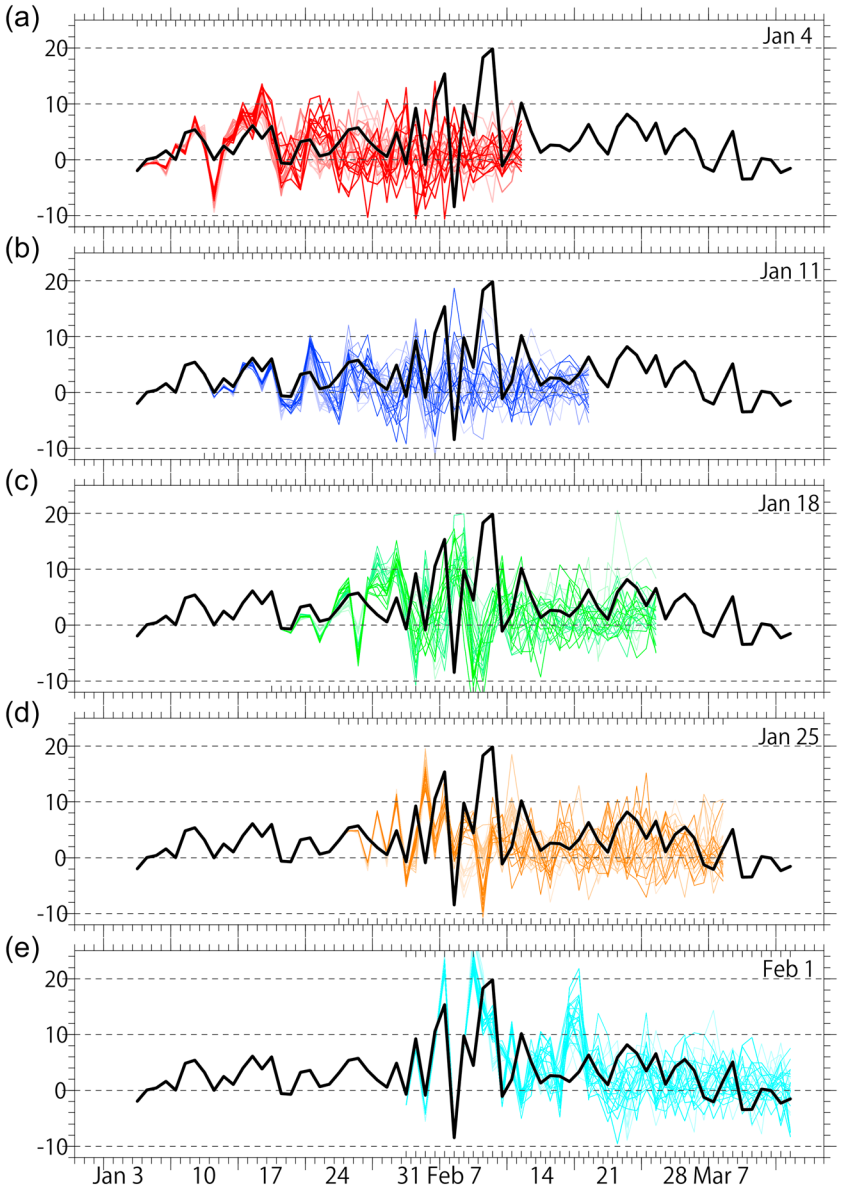

Figure 4. Time series of the zonal average eddy momentum flux ($u'v'$ in $m^2\ s^{-2}$) due to the daily averaged zonal wave number 1–20 components at 40 hPa and 10°N. The individual 27 ensemble members were plotted along with the MERRA-2 data after the same calculation (black curves). The different initial dates are indicated by colors (red: 4 January, blue: 11 January, green: 18 January, orange: 25 January, and cyan: 1 February), and the value of RHc by changing saturation (light: 0.6, medium: 0.72, and dark: 0.8).

Figures 3g and 3h show the squared refractive index for the zonal wave number 1–2 stationary planetary waves (cf. Andrews et al., 1987) as well as the E-P flux vectors for the Large-Waves, which are calculated using the ensemble mean data corresponding to Figures 3c and 3d. It is reasonable to conclude that the zonal mean structures of $\overline{u}$ (and thus n^2) in the NH subtropics during January–February 2016 form a waveguide for quasi-stationary planetary waves, focusing the southward and upward propagating NH Rossby wave components near the 40 hPa level. Waves refract toward regions of steeper positive refractive index gradient. This gradient is clearly evident at 40 hPa, and once established, the mean flow effects of the waves themselves may contribute to maintaining and enhancing the waveguide through a kind of positive feedback. Consequently, the prediction of 40 hPa equatorial $\overline{u}$ is robust.

Figure 12 in Coy et al. (2017) compares meridional structures of $\overline{u}$ during February 1988, 2011, 2014, and 2016. February 1988 most closely resembles 2016, but the center of the QBO westerly winds are shifted northward

from the equator in 1998. The waveguide structures in the lower stratosphere including the QBO itself in January–February 2016 looked already preconditioned; future research should focus on the earlier preconditioning period to explore its role in the QBO disruption.

4. Concluding Remarks

The numerical experiments conducted in this project have shown that at least the JAGUAR model with fine vertical resolution is able to successfully forecast the development of the disruption in the usual QBO equatorial wind behavior in early 2016, at least from initial conditions at and after 4 January. This stands in stark contrast to the failure of operational long-range forecasts in representing the unusual QBO behavior (Osprey et al., 2016). The difference might be a consequence of the operational models' reliance on parameterization of mean flow forcing from subgrid-scale gravity waves which tend to force very regular QBO behavior. Otherwise, it might highlight the importance of skillful prediction of SST in the operational seasonal prediction systems, while the present hindcast simulation uses the observed SST and may be strongly affected by an extreme El Niño event (Barton & McCormack, 2017). Anyways, it should be noted that the lead time of present hindcast is limited to 40 days, which is much shorter than that in the seasonal prediction results reported by Osprey et al. (2016). One big issue we are now addressing in our ongoing research is how far back successful forecasts can be initialized for this exceptional event.

The fact that the ensemble members of our hindcast all displayed fairly successful equatorial $\overline{u}$ hindcasts despite the other differences apparent among the members allows us to draw strong conclusions about aspects of the hindcasts that are not crucial for the development of and forecast of the $\overline{u}$ disruption. Notably, neither the variability of the NH stratospheric polar vortex nor the precise strength of the vertical wave E-P flux from gravity waves excited in the tropical troposphere is critical to the forecasts of equatorial $\overline{u}$ in the stratosphere.

The existence of the successful hindcasts also means that in contrast to previous studies that rely on global reanalyses, we have completely self-consistent model simulations of the disruption behavior that can be analyzed to diagnose the detailed dynamics involved. Our analysis has confirmed earlier results (Coy et al., 2017; Osprey et al., 2016) that planetary Rossby wave components propagated southward from the NH subtropics to the SH subtropics, generating the easterly wind accelerations in the SH flank of QBO westerly winds near 40 hPa, and the development of the shallow easterly wind layer (Figures 3c and 3d). The explicitly resolved vertically propagating gravity waves did not significantly generate zonal wind accelerations near 40 hPa at this time (Figures 3e and 3f).

The meridional distribution of planetary wave refractive index and the simulated E-P fluxes suggest that the meridional structures of $\overline{u}$ in the NH subtropics during January–February 2016 form a waveguide for the southward and upward propagating NH Rossby wave components, facilitating their focus and subsequent dissipation into the equatorial layer around 40 hPa.

Future hindcast studies with the JAGUAR model will address the dynamics and predictability of the development of the waveguide structures which appear to precondition the equatorial stratosphere for the easterly disruption. The results from this one model study of a particular QBO development in 2015/2016 will be placed in context with the anticipated results of a multimodel experiment to test the predictability of the QBO in other seasons and years, which is now being conducted under the aegis of the SPARC-QBOi programme (Butchart et al., 2017).

Acknowledgments

The authors would like to thank two anonymous reviewers for providing comments and suggestions, which were helpful to improve the manuscript. This study was partly supported by a Japan Science and Technology Agency (JST) as part of the Belmont Forum and by the "Integrated Research Program for Advancing Climate Models (TOUGOU program)" from the Ministry of Education, Culture, Sports, Science and Technology (MEXT), Japan. Y. K. was supported by JSPS KAKENHI grants 15KK0178, 16H04052, 17K18816, and 26287117 and by the Environment Research and Technology Development Fund (2-1503) of the Environmental Restoration and Conservation Agency, Japan. S. M. O. was funded under the Natural Environment Research Council (NERC) grant (NE/P006779/1). The numerical simulations in this study were performed using the Earth Simulator, and figures were drawn using GTOOL and the GFD-DENNOU Library. The numerical data used in this study are available from https://doi.org/10.5281/zenodo.1115407.

References

Andrews, D. G., Holton, J. R., & Leovy, C. B. (1987). *Middle Atmosphere Dynamics*, *International Geophysics Series* (Vol. 40). New York: Academic Press.

Baldwin, M. P., Gray, L. J., Dunkerton, T. J., Hamilton, K., Haynes, P. H., Randel, W. J., … Takahashi, M. (2001). The quasi-biennial oscillation. *Reviews of Geophysics*, *39*(2), 179–229. https://doi.org/10.1029/1999RG000073

Banzon, V., Smith, T. M., Chin, T. M., Liu, C., & Hankins, W. (2016). A long-term record of blended satellite and in situ sea-surface temperature for climate monitoring, modeling and environmental studies. *Earth System Science Data*, *8*(1), 165–176. https://doi.org/10.5194/essd-8-165-2016

Barton, C. A., & McCormack, J. P. (2017). Origin of the 2016 QBO disruption and its relationship to extreme el Niño events. *Geophysical Research Letters*, *44*, 11,150–11,157. https://doi.org/10.1002/2017GL075576

Boer, G. J., & Hamilton, K. (2008). QBO influence on extratropical predictive skill. *Climate Dynamics*, *31*(7-8), 987–1000. https://doi.org/10.1007/s00382-008-0379-5

Butchart, N., Anstey, J. A., Hamilton, K., Osprey, S., McLandress, C., Bushell, A. C., … Yukimoto, S. (2017). Overview of experiment design and comparison of models participating in phase one of the SPARC quasi-biennial oscillation initiative (QBOi). *Geoscientific Model Development Discussion*, *16*, 1–35. https://doi.org/10.5194/gmd-2017-187

Coy, L., Newman, P., Pawson, S., & Lait, L. R. (2017). Dynamics of the disrupted 2015–16 quasi-biennial oscillation. *Journal of Climate*, *30*(15), 5661–5674. https://doi.org/10.1175/JCLI-D-16-0663.1

Dunkerton, T. J. (2016). The quasi-biennial oscillation of 2015–2016: Hiccup or death spiral? *Geophysical Research Letters*, *43*, 10,547–10,552. https://doi.org/10.1002/2016GL070921

Emori, S., Nozawa, T., Numaguchi, A., & Uno, I. (2001). Importance of cumulus parameterization for precipitation simulation over East Asia in June. *Journal of the Meteorological Society of Japan*, *79*(4), 939–947. https://doi.org/10.2151/jmsj.79.939

Global Modeling and Assimilation Office (2015). MERRA-2 inst3_3d_asm_Nv: 3D, 3-hourly, instantaneous, model-level, assimilation, assimilated meteorological fields, version 5.12.4. GSFC Distributed Active Archive Center, accessed 1 February 2017. https://doi.org/10.5067/WWQSXQ8IVFW8

Kawatani, Y., Sato, K., Dunkerton, T. J., Watanabe, S., Miyahara, S., & Takahashi, M. (2010a). The roles of equatorial trapped waves and internal inertia–gravity waves in driving the quasi-biennial oscillation. Part I: Zonal mean wave forcing. *Journal of the Atmospheric Sciences*, *67*(4), 981–997. https://doi.org/10.1175/2009JAS3223.1

Kawatani, Y., Sato, K., Dunkerton, T. J., Watanabe, S., Miyahara, S., & Takahashi, M. (2010b). The roles of equatorial trapped waves and internal inertia–gravity waves in driving the quasi-biennial oscillation. Part II: Three-dimensional distribution of wave forcing. *Journal of the Atmospheric Sciences*, *67*(4), 981–997. https://doi.org/10.1175/2009JAS3223.1

Li, D., & Shine, K. P. (1999). UGAMP ozone climatology. In *British atmospheric data center*. Retrieved from http://badc.nerc.ac.uk/data/ugamp-o3-climatology/

Marshall, A. G., & Scaife, A. A. (2009). Impact of the QBO on surface winter climate. *Jounal of Geophysical Research*, *114*, D18110. https://doi.org/10.1029/2009JD011737

Newman, P. A., Coy, L., Pawson, S., & Lait, L. R. (2016). The anomalous change in the QBO in 2015–2016. *Geophysical Research Letters*, *43*, 8791–8797. https://doi.org/10.1002/2016GL070373

Osprey, S., Butchart, N., Knight, J. R., Scaife, A. A., Hamilton, K., Anstey, J. A., … Zhang, C. (2016). An unexpected disruption of the atmospheric quasi-biennial oscillation. *Science*, *353*(6306), 1424–1427. https://doi.org/10.1126/science.aah4156

Scaife, A. A., Athanassiadou, M., Andrews, M., Arribas, A., Baldwin, M., Dunstone, N., … Williams, A. (2014). Predictability of the quasi-biennial oscillation and its northern winter teleconnection on seasonal to decadal timescales. *Geophysical Research Letters*, *41*(5), 1752–1758. https://doi.org/10.1002/2013GL059160

Schenzinger, V., Osprey, S., Gray, L., & Butchart, N. (2017). Defining metrics of the quasi-biennial oscillation in global climate models. *Geoscientific Model Development*, *10*(6), 2157–2168. https://doi.org/10.5194/gmd-10-2157-2017

Watanabe, S., Kawatani, Y., Tomikawa, Y., Miyazaki, K., Takahashi, M., & Sato, K. (2008). General aspects of a T213L256 middle atmosphere general circulation model. *Journal of Geophysical Research*, *113*, D12110. https://doi.org/10.1029/2008JD010026

Watanabe, S., & Miyahara, S. (2009). Quantification of the gravity wave forcing of the migrating diurnal tide in a gravity wave-resolving general circulation model. *Journal of Geophysical Research*, *114*, D07110. https://doi.org/10.1029/2008JD011218

Watanabe, S., Sato, K., Kawatani, Y., & Takahashi, M. (2015). Vertical resolution dependence of simulated gravity wave flux simulated by an atmospheric general circulation model. *Geoscientific Model Development*, *8*, 1637–1644. https://doi.org/10.5194/gmd-8-1637-2015